ACS OMEGA

http://pubs.acs.org/journal/acsodf

Article

Ambient Temperature Affects Protein Self-Assembly by Interfering with the Interfacial Aggregation Behavior

Han-Zhang Mou, Cong-Lin Zhao, Juan Song, Lei Xing,* Hong-Yuan Chen, and Jing-Juan Xu*

Cite This: *ACS Omega* 2023, 8, 24999−25008

Read Online

ACCESS | Metrics & More | Article Recommendations | Supporting Information

ABSTRACT: Amyloid fibrillation is known to be associated with degenerative diseases, and mature fibrils are also considered as valuable biomedical materials. Thus, the mechanism and influencing factors of fibrillation have always been the focus of research. However, in vitro studies are always plagued by low reproducibility of kinetics and the molecular mechanism of amyloid fibrillation is under debate until now. Here, we identified the ambient temperature (AT) as a non-negligible interfering factor in in vitro self-assembly of globular protein hen egg-white lysozyme for the first time. By multimodal molecular spectroscopy methods, not only the effect of ATs on the kinetics of protein aggregation was described but also the conformational changes of the molecular structure with different ATs were captured. Through investigating the dependence of interfacial area and catalysis, the reason for this influence was construed by the various aggregation behaviors of protein molecules in the two-phase interface. The results suggest that in vitro mechanism research on protein fibrillation needs to first clarify the AT for a more accurate comparative analysis. The proposal of this concept will provide a new clue for a deeper understanding of the mechanism of protein self-assembly and may have an impact on evaluating the efficiency of amyloid accelerators or inhibitors based on the comparative analysis of protein self-assembly.

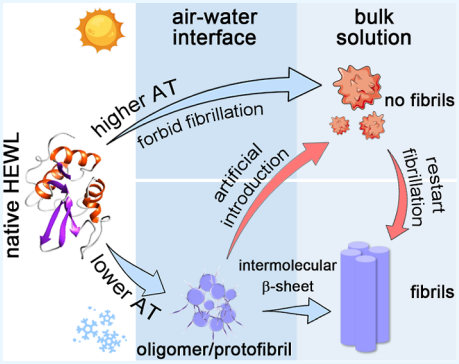

INTRODUCTION

Amyloid fibril is a frequently mentioned type of supramolecular structure, resulting from the self-assembly of soluble peptides and proteins, which plays a crucial role in many life activities and functions.[1−4] They were initially identified in the pathology and thought to be related to degenerative diseases.[5,6] The nanostructure of amyloid fibrils presents as elongated and unbranched fibrils of several nanometers in diameter and several micrometers in length with numerous intermolecular β-sheet patterns.[6−8] Nowadays, considering the natural biocompatibility and the nanoscale topography, amyloid fibrils are considered one of the valuable nanomaterials and have broad applications in biomedical, biomaterial, and nanotechnology fields.[2,3,9] Therefore, for effective therapy of degenerative disease and design of functional biomaterials, it is of great significance to explore different fibril-forming conditions and obtain the precise fibrillation mechanism.

In the research on protein fibrillation, globular protein hen egg-white lysozyme (HEWL) is always mentioned due to its abundant resources. It shares 60% sequence identity with human lysozyme that causes hereditary systemic amyloidosis.[10] The mature fibrils of HEWL possess rigidity, chemical stability, and high aspect ratio, which are well known for the design of enzymatically active hydrogel particles or drug carrier hydrogels.[10−12] Accordingly, the relevant results obtained from the study on HEWL are of reference value for most protein self-assembly research.[10,13] Considering the complexity and variability of the in vivo environment, abundant in vitro experiments connected with lysozyme fibrillation are being carried out. To date, many factors, such as concentration, solution temperature, pH, pressure, radiation, stirring rate, small molecules, and the surface or interface, have been identified to affect protein fibrillation in vitro.[4,14,15] Although these parameters have been controlled, it remains challenging to upward the precise repeatability of amyloid fibrillation kinetics between laboratories as amyloid fibrillation is a highly sensitive process, such as the inconsistent kinetic fluorescent curves and the quite stochastic mature fibrils.[4,16,17] Accordingly, the exact molecular mechanism of amyloid fibrillation is still under debate. This will be very detrimental to drug screening assays targeting the treatment of neurodegenerative diseases. Many groups made considerable efforts to find potential reasons for the above phenomenon. Ramamoorthy's group pointed out that the irreproducibility of many results partially stymied understanding of the fibrillation process. They showed the formation of micelle-like oligomers at specific critical concentrations and temperatures may contribute to this phenomenon.[18] Shanmugam's group emphasized

Received: March 9, 2023
Accepted: June 22, 2023
Published: July 7, 2023

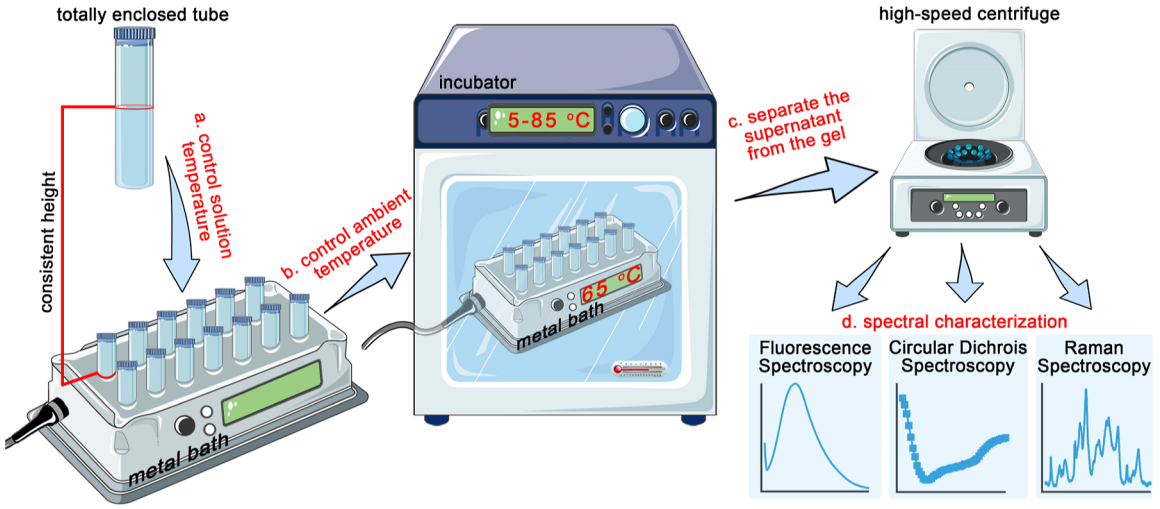

Figure 1. Experimental procedure at a stable solution and controllable AT.

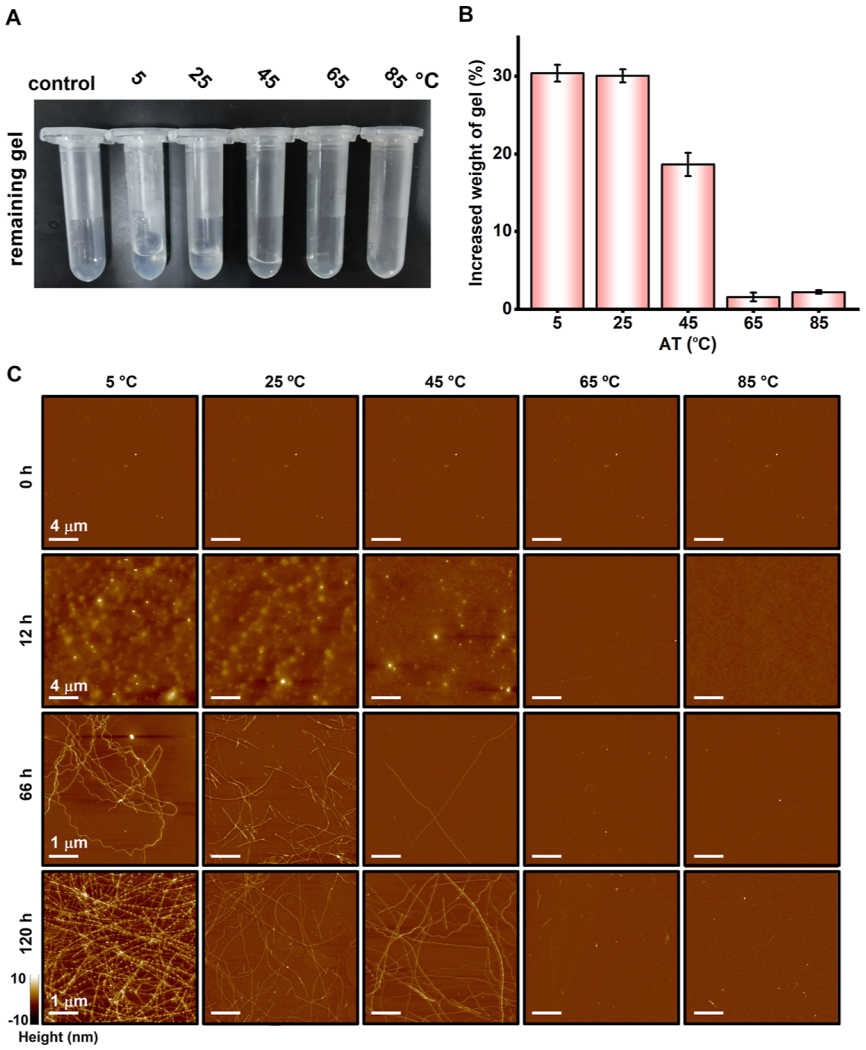

Figure 2. Morphology of HEWL with different ATs. Physical map (A) and weight change (B) of remaining hydrogels in the test tubes after 120 h of incubation with different ATs. (C) AFM images of HEWL at different incubation times with various ATs (5, 25, 45, 65, and 85 °C).

the influence of different air−water interfacial areas on the precise repeatability of amyloid fibrillation kinetics and found that the larger interfacial area can effectively promote the formation of fibrils.[19] Knowles's group further revealed that the increasing surface-to-volume ratio of the air−water interface can also accelerate the protein self-assembly process.[20] These studies suggested the importance of discovering the unknown influencing factors of protein fibrillation in laboratory experi-

https://doi.org/10.1021/acsomega.3c01606
ACS Omega 2023, 8, 24999−25008

ments. It prompts us to think about whether there are still unconsidered contributing factors or fibrillation mechanisms.

Although the effect of solution temperature has been proposed for a long time, the unavoidable influence of ambient temperature (AT) on protein fibrillation is always neglected in in vitro research. Here, we report for the first time that the AT can obviously affect the in vitro self-assembly of globular protein HEWL. Through multimodal molecular spectroscopy methods, the inconsistent kinetic processes of HEWL fibrillation with different ATs were captured from the molecular structure level. The higher AT not only delays the unfolding of the tertiary structure but also inhibits the formation of the intermolecular β-sheet structure. Investigation on the dependence of interfacial area and catalysis further revealed the probable reason for the influence of AT on fibrillation, resulting from the different aggregation behaviors of protein molecules at the air−water interface. Our results showed that AT was one of the influencing factors that cannot be ignored in the self-assembly of globular protein HEWL in vitro. This will remind us to pay attention to the role of AT in vitro mechanism research of fibrillation. The relevant results may also be extended to other globular proteins.

RESULTS AND DISCUSSION

Control of Solution and Ambient Temperature. The influence of different solution temperatures on fibrillation kinetics has been widely studied. Heating (65 °C) and acidic conditions (pH 1∼2) are believed to effectively accelerate the fibrillation process of HEWL in the laboratory.[13,21,22] Under this condition, it has been confirmed that HEWL can form aggregates with different morphologies at various stages of incubation.[5,23,24] Typically, the oligomer with a nanometer size and nearly spherical morphology can be concentrated in the very early stage. Following, some short fiber-like aggregates with several micrometers in length and several nanometers in height were generated, called protofibril. Finally, mature fibrils can become abundant, ranging from tens to hundreds of microns in length.

To ensure a stable solution temperature and controllable AT during protein fibrillation, we proposed a reliable experimental protocol. As shown in Figure 1, the equivalent protein aqueous solution (pH ∼ 2) was sealed in several enclosed tubes and heated by a metal bath. The height of the air−water interface in the test tube was consistent with the height of the metal bath. The metal bath was set at a constant temperature (65 °C). Then, the AT was controlled by an incubator inside which the aforementioned metal bath was placed. The temperature of this incubator was adjustable from 5−85 °C. Meanwhile, a thermometer is also used to monitor the actual temperature inside the incubator. After incubating at different times, the test tubes including the protein sample were taken out and the supernatant was separated from the hydrogels by a high-speed centrifuge. Finally, multimodal molecular spectroscopy was utilized to track the structural variety of proteins in the supernatant. Herein, the whole spectral features of proteins or aggregates can be captured since part of the hydrogels and fibrils remain suspended in the supernatants at the centrifugal speed and time used in this work.[24,25]

Characterization of the Morphology of HEWL. HEWL fibrils can be designed with multiple supramolecular structures under different in vitro conditions.[22,26,27] To evaluate the impact of AT, the morphology of HEWL during fibrillation was characterized under different incubation conditions. As shown in Figure 2A, after 120 h incubation, large amounts of hydrogels formed under incubation with ATs of 5, 25 , and 45 °C. Specifically, the lower the AT was, the more hydrogels could be formed (Figure 2B). This visual evidence did prove the obvious effect of ATs on protein self-assembly. Then, atomic force microscopy (AFM) was employed to capture protein morphological changes in detail. Figure 2C showed the AFM morphology of HEWL incubated with various ATs at different times. The morphological changes of HEWL mainly experienced three stages with ATs of 5, 25, and 45 °C. The native HEWL was almost invisible on the surface of the mica. After heating for ∼12 h, the spherical oligomers were formed. For the next 50 h of continuous heating, the oligomers gradually grew into protofibrils or mature fibrils. Then, more and more mature amyloid fibrils with a length of several microns appeared after 120 h of incubation, which was consistent with previous studies.[24,28,29] Meanwhile, the largest number of oligomers or fibrils was also observed with 5 °C of AT regardless of the incubation time, and the mature fibrils had an obvious periodic structure with ∼147 nm of pitches (Figure S1A). In contrast, with 65 and 85 °C of ATs, almost no mature protein fibrils were in sight on the surface of the mica even after 120 h heating, suggesting that the fibrillation process of HEWL was significantly slowed.

The sizes of aggregates in each incubation condition were also analyzed from AFM results and shown in Figure S1. Herein, the height was considered as a more immediate parameter to evaluate the growth process of aggregates, rather than the width relying on the geometry of the tip.[30] From Figure S1B, we can see that with the increase of ATs from 25 to 45 °C, the height of the early-formed oligomers gradually increased (12 h), while the height of the subsequently-formed protofibrils and mature fibers decreased (66 and 120 h). Due to almost no oligomer formation at 12 h of incubation with 65 and 85 °C ATs, the particle size obtained on the surface of mica sheets was identical to the 0 h. Interestingly, the changing trend of each AT except 85 °C over time was very similar (Figure S1C). They all went through a process of first increasing and then decreasing in size from 0 to 120 h incubation. Only an upward trend was observed with 85 °C AT, which is reasonable because even after 120 h of incubation, the protofibrils or mature fibers were almost invisible. These results supported the abovementioned view on the obvious influence of ATs on the fibrillation process of HEWL. To explore its influence mechanism directly from the molecular level, we chose two of the abovementioned ATs for the following experiments and discussions, which were 25 °C (lower AT) and 65 °C (higher AT).

AFM images can provide intuitive feedback on changes in protein morphology, while dynamic light scattering (DLS) experiments can further capture the average size mutation of aggregates in the aqueous phase. A 0.22 μm filter membrane was employed to filter the supernatant, which can minimize the ineluctable size interference from extremely long mature fibers as much as possible. As seen in Figure S2, the lower AT significantly promoted the growth of HEWL aggregates, the size of which increased from ∼0.1 to ∼30 nm after continuous heating for 120 h. With the higher AT, protein size only increased from ∼0.1 to ∼0.12 nm after heating for 120 h. This result implied that the higher AT can slow down the formation of the aggregates, which further supported the above-mentioned view on the delaying effect of higher AT on protein aggregation.

https://doi.org/10.1021/acsomega.3c01606
ACS Omega 2023, 8, 24999−25008

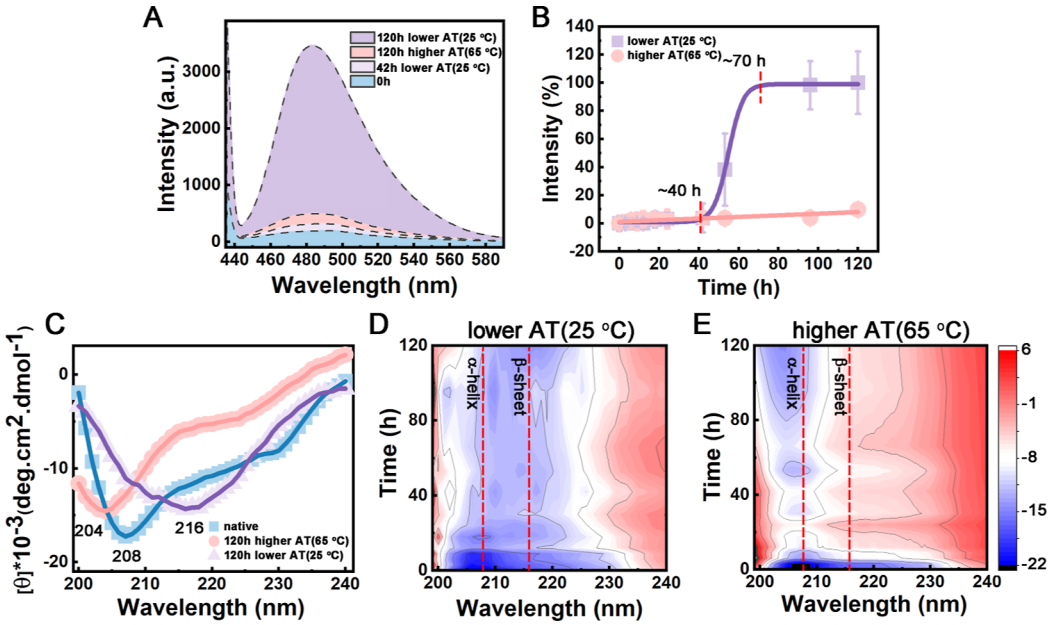

Figure 3. Characterization of protein structure with lower and higher AT by fluorescence and CD spectroscopy. (A) ThT fluorescence of HEWL at different incubation times with lower AT and higher AT. (B) Comparison of ThT fluorescence kinetic curves with lower AT (purple) and higher AT (red). (C) CD spectra of HEWL at 0 h (blue) and 120 h of incubation time with lower AT (purple) and higher AT (red). Two-dimensional CD spectra of HEWL during different incubation times with lower AT (D) and higher AT (E).

Measurement of the Molecular Structure of HEWL. To capture the changes in the molecular structure of proteins affected by the different ATs, multimodal molecular spectroscopy methods were employed to detect protein fibrillation dynamic processes. Thioflavin T (ThT), a small fluorescent dye molecule, was pre-tagged with the protein HEWL to track the intermolecular structure of the protein. The stronger the ThT fluorescence intensity is, the more intermolecular β-sheet structures there are, which indicates the formation of mature fibers.[31−33] Figure 3A showed that with the lower AT, the fluorescence intensity gradually increased with the incubation time. After 120 h of incubation, the intensity reached approximately 3500. Nevertheless, the fluorescence intensity grew little with the higher AT. The comparison of fluorescence kinetic curves was also shown in Figure 3B. As described in previous works,[34−36] the kinetic curves can be fitted according to the following formula to obtain the specific time experienced based on the incubation time

$$I = I_D + (I_N - I_D)/[1 + \exp[-(T - T_m)/\Delta T]]$$

in this work, I_N and I_D are the initial and final values of fluorescence intensity, Raman shift, or full width at half maximum (FWHM) of Raman peak. T_m is the midpoint value obtained by curve fitting, and 2 × ΔT is the time corresponding to the curve growth stage. Through this formula, we can obtain the lag duration (T_0) and equilibrium duration (T_e) of kinetic curves of fluorescence intensity or Raman markers under different incubation conditions.

After fitting, the fluorescence kinetic curve of HEWL fibrillation presented a typical S-shaped curve with the lower AT, suggesting that protein fibrillation mainly has gone through three phases (lag phase, growth phase, and equilibrium phase). It can be seen that the formation of the intermolecular β-sheet structure occurred at ∼ 40 h and then reached equilibrium after ∼70 h incubation. However, as shown in Figure 3B, the kinetic curve of fluorescence intensity was almost linear with the higher AT. Figure S3 showed that the higher AT can induce a longer lag phase. The ThT fluorescence results indicated that intermolecular β-sheet structures were not formed abundantly in the HEWL fibrillation with the higher AT, which is the structural basis of the mature fibers. Moreover, the extended time of lag phase further revealed that higher AT may delay or prevent the nucleation process.

Apart from the ThT fluorescence spectroscopy to investigate the intermolecular structure of the protein, far-UV circular dichroism spectroscopy (CD) was often mentioned to monitor the alteration of protein secondary structures. As shown in Figure 3C, the spectrum of native HEWL displayed a minimum at ∼208 nm, which is the characteristic feature of α-helix-rich conformation.[28,37] After 120 h incubation with lower AT, the negative ellipticity of the peak at ∼208 nm had a significant decrease and a deep peak at ∼216 nm was raised, indicating the formation of a β-sheet structure.[28] However, this shape variation of the spectrum was not observed with the higher AT. The two-dimensional CD spectra of HEWL with lower and higher AT are also shown in Figure 3D,E, which exhibited time-dependent distinctions. With the lower AT, the peaks with the negative ellipticity corresponding to the blue area of Figure 3D first had a blueshift before ∼40 h incubation, and then, a redshift has occurred. On the contrary, the peaks with the negative ellipticity corresponding to the blue area of Figure 3E were always blue-shifted during 120 h of incubation with the higher AT. These results further validated the influence of AT on protein fibrillation.

Taking advantage of the strong responses on protein side chains and backbone groups simultaneously, Raman spectroscopy is also chosen to directly track changes in the tertiary and secondary structure during HEWL fibrillation.[38−41] Figure S4 shows the whole Raman spectra of the native protein and the protein after 120 h of incubation with the different ATs. We can see that many peaks in the Raman spectra were

https://doi.org/10.1021/acsomega.3c01606
ACS Omega 2023, 8, 24999−25008

significantly different, such as the tyrosine ring modes at 828 and 853 cm^{-1}, the N−C−C stretch at 935−945 cm^{-1}, or the amide III at 1225−1275 cm^{-1}, which suggested that there are obvious structural differences between these proteins.[38,42]

Two relatively independent peaks at 759 and 1658 cm^{-1} were selected for dynamic analysis of the structural variation of the protein. Here, considering the heterogeneity of sample preparation, Raman intensity is not a parameter for dynamic analysis. The position and full width at half maxima (FWHM) of Raman peaks are inherent properties of the molecule, which are only dependent on conformational changes caused by external environmental interference, rather than sample preparation, so they can be directly applied for dynamic analysis.[38]

The Raman peak at 759 cm^{-1} is mainly attributed to the coupling vibration of the symmetrical loop respiration of benzene and pyrrole on the tryptophan (Trp) residue.[40,43] After 120 h of incubation, the FWHM of the peak broadened, and the position of the peak had a redshift regardless of lower AT and higher AT (Figure 4A), indicating a conformational

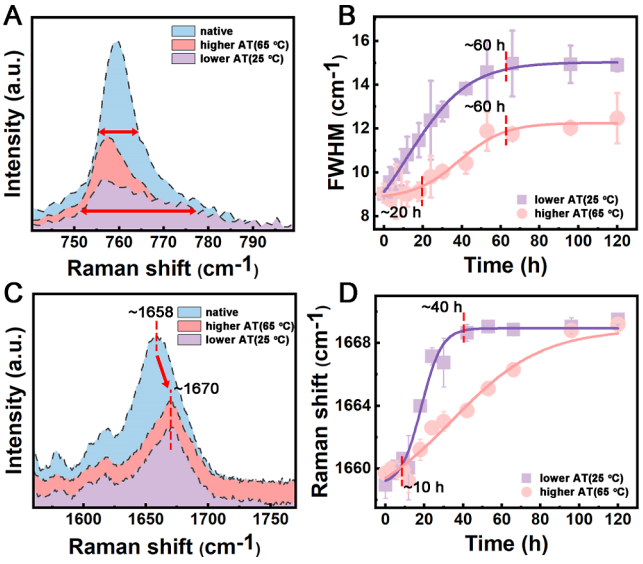

Figure 4. Characterization of the protein structure with lower and higher AT by Raman spectroscopy. Raman spectra comparison of Trp (A) and amide I (C) between the native state (blue) and after 120 h incubation with lower AT (purple) and higher AT (red). Raman FWHM kinetic curves of Trp (B) and Raman shift kinetic curves of amide I (D) with lower AT (purple) and higher AT (red).

change of Trp from being relatively fixed to more diversified and an expanding interaction between the Trp side chain residues and the surrounding microenvironment.[44] It also implied the unfolding of the protein tertiary structure. The kinetic curves of the Trp peak in Figure 4B showed that the FWHM rapidly widened from ~9 to ~15 cm^{-1} with the lower AT and reached equilibrium in approximately ~60 h without the lag phase. However, with the higher AT, the FWHM of Trp residue only broadened from ~9 to ~12 cm^{-1}. The kinetic curve was obviously slowed down and the lag phase lasted for nearly ~20 h.

The Raman peak at 1658 cm^{-1} is assigned as the amide I group in the protein, which is mainly composed of the coupling mode of C═O and C−N tensile vibration and a small part of N−H in-plane bending vibration.[38] The native state of HEWL mainly contains a large amount of α-helical structure, which makes the Raman shift of the amide I group locate at a lower wavenumber (~1658 cm^{-1}), and the formation of protein aggregation will lead to the peak of the amide I group to blueshift.[38] We did observe a blueshift of the amide I peak with the increase in incubation time, whether with lower or higher ATs, which indicated a translation of the skeleton structure (Figure 4C). Interestingly, the distinguishable kinetic curves of the amide I peak under two conditions can be observed in Figure 4D. It showed that HEWL fibrillation did not completely reach equilibrium until 120 h of incubation with the higher AT, the growth phase of which was much slower than that with the lower AT. Here, we observed that the final peak positions under the two conditions were very close. However, it can be confirmed that by combining the results of fluorescence and CD spectra (Figure 3), the intermolecular β-sheet structures were barely formed in the higher AT condition. Additionally, the rise of the peak at 1628 cm^{-1} in the infrared spectra is a fingerprint of intermolecular β-sheet structure formation.[34,45,46] This characteristic peak was obvious with the lower AT, but it was almost invisible with the higher AT (Figure S5). These pieces of evidence showed that although the final peak positions of amide I were similar under the two conditions, the skeleton structures were obviously inconsistent. As previously described, this broad spectral peak of amide I is mainly the contribution of the superposition of many detailed structures, especially within the high wavenumbers of Raman spectra, including β-trans, β-sheet, random coil, etc.[47,48] These structures also shared part of spectral segments with each other. Consequently, a similar peak location was possible due to the different contents of these secondary structures. Collectively, we concluded that higher AT not only inhibited the unfolding of tertiary structure but also induced the most α-helical structure of HEWL to convert into other structures rather than the intermolecular β-sheet. This protein state was completely different from the mature fibril state, called the denaturation state by us in the following discussion.

Protein Aggregation Behavior at the Two-Phase Interface. After capturing the distinctive conformational changes under different ATs, we attempted to clarify the origin of the observed effects. One contribution that can be considered is the temperature gradient between the sample solution with tube or environment, which may cause turbulent motions in the tubes to affect the results. From Figure S6A, we clearly saw a temperature gradient between the sample solution with tube or environment under 5 °C AT. Fortunately, given different incubation times, it seemed that this temperature gradient remained almost stable after 12 h of incubation. To evaluate the impact of this temperature gradient, we designed a control experiment as shown in Figure S6B. Different from the conditions used in Figures 2 or S6A, the three test tubes were filled with aqueous solutions of protein and the air−water interface did not exist. The height ratios of protein solutions extending and immersing ($H_{ex/im}$) in the metal bath were 1:1, 1.5:1, and 2:1, respectively. Apart from these distinctions, the other parameters were consistent with the above mentioned in Figure 2, including temperatures of ambient (5 °C) and metal bath (65 °C), protein solution concentration (20 mg/mL), pH (~2.0), etc. Under this condition, the temperature gradient layers with different sizes can be formed in both the test tube and the aqueous solution even without the air−water interface (Figure S6C). Obviously, the higher the $H_{ex/im}$ values, the larger the temperature gradient sizes (TGSs). The slight

https://doi.org/10.1021/acsomega.3c01606
ACS Omega 2023, 8, 24999−25008

denaturation of the temperature gradient layer in Figure S6C was possibly due to the turbulent motions of protein solutions in the tubes. Unfortunately, despite the assistance of this maximum TGS observed in c of Figure S6C, the protein aggregates were barely identified in the absence of an air−water interface. It can be concluded from the almost constant intensity of ThT fluorescence (Figure S6D) and the sample photos after centrifugation (Figure S6E). Meanwhile, the AFM images of proteins with no fibrils after 120 h of incubation also intuitively supported this viewpoint (Figure S6F). These results indicated that the temperature gradient did not play a major role in interfering with the fibrillation process under the above-mentioned incubation conditions in this work.

In the beginning, we mentioned that large quantities of hydrogels appeared after HEWL incubation with the lower AT (Figure 1A). In fact, these hydrogels can be visible to the naked eye at the very early time of HEWL incubation with the lower AT. To show these early-formed hydrogel samples more clearly, protein incubation was also performed on the glass vials with the larger size. As shown in Figure S7A,B, the hydrogels appeared after ∼24 h of incubation and adhered to the glass vial around the air−water interface. Conversely, the hydrogels were not observed whether in an aqueous solution or on the bottle wall even after 120 h incubation with the higher AT. The morphology of hydrogels characterized by AFM showed that part oligomers (marked by red circles) and protofibrils (marked by red arrowheads) were contained in (Figure S8A). ThT fluorescence spectra and Raman spectra also confirmed that these hydrogels were rich in intermolecular β-sheet structures (Figure S8B,C). This phenomenon is reasonable because a great number of previous literatures witnessed the effect of the air−water interface on protein fibrillation. The enriched oligomers and protofibrils at the air−water interface will further induce the secondary nucleation of the protein in the bulk solution, thereby catalyzing the entire protein fibrillation process.[49,50] Thereby, it is easy to associate that the AT may interfere with the aggregation behavior of protein molecules at the air−water interface, which further leads to the different dynamics of protein fibrillation in the solution phase.

To highlight the role of the air−water interface in the fibrillation process, we designed three strategies (a, b, and c) for comparative analysis. As shown in Figure 5A, the heights of the air−water interfaces were the same in a and b, while the volume of protein solution and interfacial area in a were larger than that in b. The interfacial area of b was the same as that of c while the height of air−water interface in c was higher than that in b and the volume of protein solution in c was the same as that in a. By comparing these three strategies in pairs, we can preliminarily determine the impact of the air−water interface on the fibrillation process. Actually, the dependence of the air−water interfacial area based on a similar volume of protein solution has been examined by Shanmugam's group, and they proposed that the larger interfacial area can effectively promote the formation of fibrils.[19] Our results supported their view, which can be concluded from the comparison of results between a and c (Figure 5B−D). Meanwhile, a larger surface-to-volume ratio (S/V) was more conducive to the fibrillation process by comparing the results of b and c (Figure 5B−D), which was also consistent with the view of Knowles's group.[20] Remarkably, we ensured uniform interfacial heights in strategies a and b, which meant that the inconsistency in S/V mainly came from the contribution of the interfacial area.

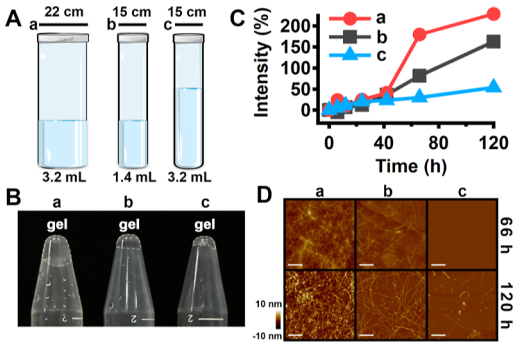

Figure 5. (A) Scheme of three strategies for comparative analysis of proteins fibrillation in different areas of the air−water interface. (B) Remaining samples separated by centrifugation after protein incubation for 120 h in the three strategies corresponding to the a, b, and c of A. (C) ThT fluorescence kinetic curves of different samples in the three strategies corresponding to the a, b, and c of A. (D) AFM images of proteins after 66 and 120 h of incubation in the three strategies corresponding to the a, b, and c of A.

Although the volume of protein solution in a was much larger than that in b, the amount of hydrogel generated (Figure 5B), the fluorescence kinetics rate (Figure 5C), or the number of mature fibers (Figure 5D) all showed that the three strategies met the order of $a > b > c$. These results first verify the contribution of the air−water interface.

To further appraise whether the hydrogels produced at the air−water interface can affect the fibrillation dynamics in the bulk solution, we embedded a certain concentration of hydrogels sample into the HEWL aqueous solution for co-incubation (with hydrogels under the higher AT), and the topography or kinetic curves were also measured by AFM, ThT fluorescence, and Raman spectroscopy at a different time (Figure 6). After adding the hydrogels sample to the culture, a large number of mature fibers formed after HEWL incubation for 42 h even with the higher AT (Figure 6A). The kinetic curves also showed that the fibrillation process was significantly accelerated. On the one hand, the kinetic curve of ThT fluorescence intensity was similar to that with lower AT (Figures 6B and 3B). On the other hand, due to the disappearance of the lag phase of secondary and tertiary structures, the equilibrium phases of the kinetic curves on Raman shift or FWHM were quickly achieved after ∼30 and ∼40 h, respectively (Figure 6C,D). However, there was still no hydrogel-like formation at the interface or in the solution phase after 120 h of incubation, as shown in Figure S9.

As we mentioned above in the multimodal molecular spectroscopy experiments, a higher AT can delay or prevent the nucleation process of protein fibrillation. Here, we directly skipped the nucleation process by artificially introducing the hydrogels into the bulk solution. Then, the protein fibrillation can be restarted and effectively catalyzed in bulk solution without any effect of higher AT. Taken together, the above results proved that AT mainly interfered with the protein aggregation behaviors at the two-phase interface to directly determine the occurrence of nucleation process and further affect the fibrillation dynamics of protein molecules in the bulk solution. Remarkably, our data do not affirm whether the fibrillation process will be significantly affected when increasing TGS by further lowering the AT. A more detailed study needs to be performed in future work based on high-resolution thermal imaging or sum frequency generation spectroscopy

https://doi.org/10.1021/acsomega.3c01606
ACS Omega 2023, 8, 24999−25008

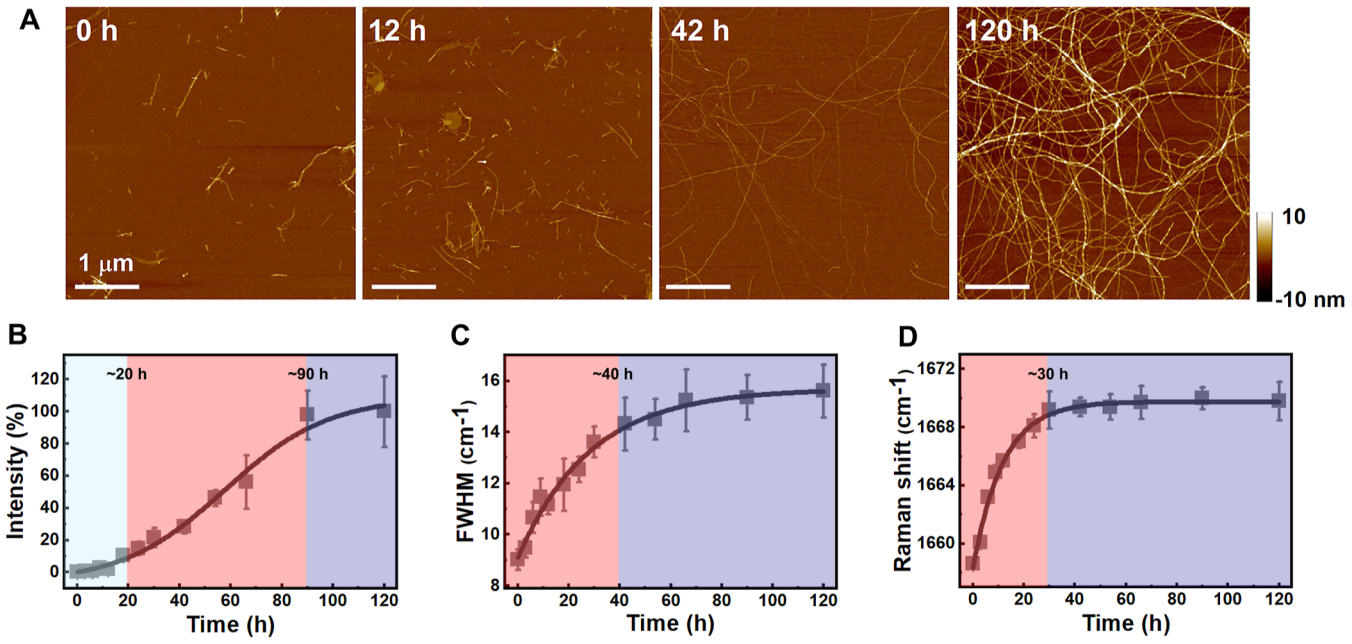

Figure 6. Verification of protein secondary nucleation catalyzed by the hydrogel. Morphology of HEWL (A), ThT fluorescence kinetic curve (B), Raman FWHM kinetic curve of Trp (C), and Raman shift kinetic curve of amide I (D) after HEWL and hydrogels co-incubation with higher AT.

Scheme 1. HEWL Fibrillation Kinetic Process with Lower AT (A) and with Higher AT (B) and after Hydrogels Coincubation with Higher AT (C).

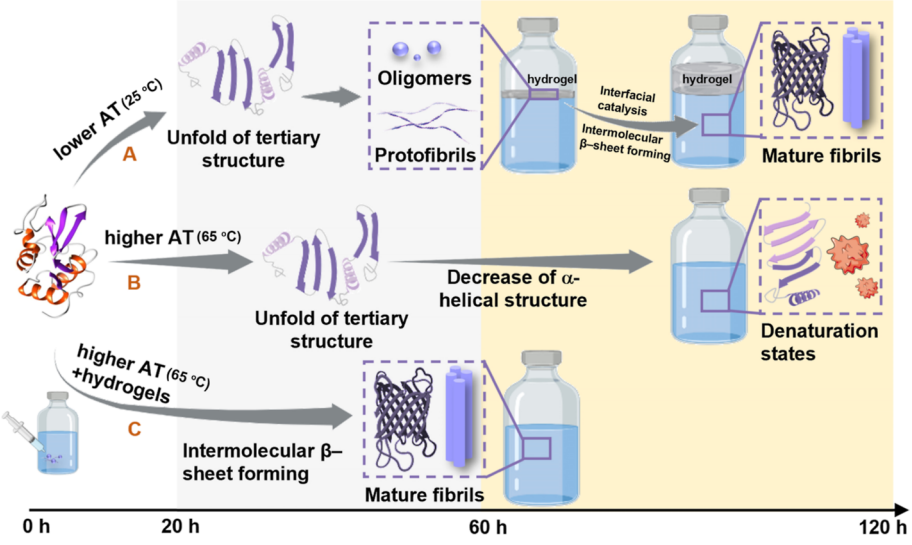

methods. Nonetheless, herein the contribution of the air−water interface to the protein fibrillation was clear.

Mechanism Diagram of Influence of Ambient Temperature on Protein Aggregation. Based on the whole experimental results, we presented a mechanism diagram of the influence of AT on protein aggregation, as shown in Scheme 1. The lower AT (A) first induced abundant hydrogels comprising oligomers and protofibrils to enrich at the air−water interface after ∼20 h of incubation. Then, these hydrogels further catalyzed the fibrillation process of protein molecules in the bulk solution phase. After ∼60 h of incubation, plentiful mature fibrils were generated in the solution. Conversely, the higher AT (B) can disturb the aggregation behaviors of protein molecules and hinder the formation of hydrogels at the air−water interface. The prohibition of this key rate-limiting step further constricted the unfolding of the tertiary structures and the conformational transformation of the α-helix structures. Even after 120 h of incubation, only denaturation state of proteins was formed in the bulk solution rather than mature starch fibers containing intermolecular β-sheet structures. When the hydrogels were artificially introduced to the bulk solution and co-cultured with the HEWL with the higher AT (C), the HEWL fibrillation process will be triggered again and the mature fibrils can be concentrated in the bulk solution after ∼40 h of incubation. Nevertheless, no hydrogel formation was observed at the air−water interface even after 120 h incubation.

https://doi.org/10.1021/acsomega.3c01606
ACS Omega 2023, 8, 24999−25008

CONCLUSIONS

Based on the above results, we believe that AT is one of the non-ignorable factors for in vitro experiments to influence the process of protein self-assembly. It can interfere with the aggregation behaviors of protein molecules at the air−water interface to further affect the fibrillation dynamics of protein molecules in the bulk solution phase. From the research on the molecular level, we know that the higher AT not only delays the unfolding of the tertiary structure of proteins but also inhibits the conversion of the secondary structure of the protein from the α-helical structure to the intermolecular β-sheet structure. The identification of such an effect further uncovers the probable reason for the low reproducibility of fibrillation kinetics in vitro experiments because the disturbance of AT will also cause a change in protein fibrillation dynamics, even if ensuring a relatively consistent solution environment. These results also reminded us to affirm the AT first when carrying out the dynamic comparative analysis of protein fibrillation in the future. This work sheds light on a deeper understanding of the protein fibrillation mechanism.

METHODS

Materials and Reagents. HEWL from hen egg white was purchased from Biotech Co. Ltd (Shanghai, China) and was used without further purification. ThT was purchased from Jiangsu Keygen Biotech Corp., Ltd (Nanjing, China). Potassium bromide was purchased from Nanjing Chemical Reagent Co., Ltd (Nanjing, China). Hydrochloric acid was purchased from Sinopharm Chemical Reagent Co., Ltd (Shanghai, China).

Preparation of HEWL Fibrils. The HEWL fibrils were prepared as mentioned before.[24,35] In short, the concentration of HEWL in the aqueous solution was 20 mg/mL, and hydrochloric acid was added to adjust the pH to ∼2.0. The same amount of solution was sealed in test tubes or glass vials and incubated at 65 °C of solution temperature without stirring. Meanwhile, the ATs were set as 5, 25, 45, 65, and 85 °C, respectively. Details of the methodology for controlling solution temperature and AT were explained in the Results and Discussion. After different incubation times, aliquots of the protein solution were taken from the tubes, and the hydrogel was separated by centrifugation at 12,000 *g* for 20 min. Finally, the aliquot supernatant was used for AFM, DLS, fluorescence measurement, CD, infrared, and Raman spectroscopy experiments. The initial protein concentrations used in all the present experiments were the same as 20 mg/mL in the aqueous solutions. However, owing to the formation of the insoluble gelatinous phase, only the soluble fraction was used in the above-mentioned experiments. The protein concentrations in the aliquot supernatant were much lower than the initial value, and they continuously decreased with the gradual increase of hydrogel at various incubation times.[29,36,39] Thus, when we compared the CD and Raman spectra at various times, the position or full width at half maxima (FWHM) of peaks were considered as parameters for dynamic analysis, rather than the intensity. Both of them are inherent properties of the molecule, which are dependent on conformational changes caused by external environmental interference. Additionally, the reported Raman spectra were accumulated and averaged by 60 acquisitions, which makes them have high reliability. For IR spectra, the protein solution was freeze-dried for infrared detection. Three independent incubation experiments with different ATs were performed for all measurements, which further ensured the reliability of the results. In reality, both the morphological changes of HEWL and the typical S-shaped curve with the lower AT were consistent with the results previously reported at room temperature.[5,15,35]

Measurement of Fiber Morphology by AFM. All the protein solution used in the AFM experiment was the 50-fold diluted supernatant with Milli-Q water after centrifugation. Then, 25 μL of diluted supernatant was dropped on the surface of a clean mica sheet and it was kept for 15 min. After the protein was adsorbed on the mica sheet, the remaining protein was rinsed with 50 μL of deionized water three times. Finally, the mica surface was dried overnight in a vacuum desiccator at room temperature. All AFM images were obtained on the Bruker ICON atomic force microscope system (Bruker, American) and 20 × 20 or 5 × 5 μm^2 scanning interfaces were used with a step size of 512 nm/pixel. The AFM images were analyzed by the open-access software NanoScope Analysis 1.8.

Measurement of Particle Size by DLS. DLS data were recorded on a NanoBrook 90plus PALS granulometry (Brookhaven, America). The supernatant was filtered with a 0.22 μm filter membrane to avoid a possible size error coming from the interference of mature fibers with several micron lengths and then added to a plastic cuvette. Each sample was measured three times at 25 °C.

Measurement of Fluorescence Spectra. Steady-state fluorescence emissions of the ThT dye (1×10^{-5} mol/L) were measured on a Hitachi F-7000 spectrofluorometer (Hitachi, Japan) within a wavelength range of 400−800 nm. 200 μL aliquots of the supernatant were picked up from vials after various incubation times and were added to 4800 μL of ThT solutions in different test tubes. For a sufficient reaction of the ThT dye and proteins, the test tubes needed to be shaken for 20 min in a dark environment. Then, the fluorescence assays of the solutions were performed three times. The excitation wavelength was 420 nm, and the intensity of the fluorescence peak at an emission wavelength of 485 nm was used for kinetic statistics. All measurements were performed under ambient conditions.

MEASUREMENT OF CD SPECTRA

CD measurements were performed on an Applied Photophysics Chirascan (Applied Photophysics, UK). Far-UV CD spectra were recorded with a step size of 1 nm and a single data sampling time of 0.8 s. CD spectra were scanned over the wavelength range of 180−260 nm in a cuvette of 0.5 cm path length. Every spectrum was taken as the average of two scans.

Measurement of Raman Spectra and Infrared Spectra. The surface-enhanced Raman spectra measurement was performed on a Renishaw inVia-Reflex Raman spectrometer with a Leica microscope (Leica, German) equipped with a 488 nm excitation laser, and a microscope with a 50× objective lens. The Raman shift was ranged from 400 to 1800 cm^{-1} and carefully calibrated using standard spectral lines from a mercury lamp. The acquisition time for each measurement was 1.2 min, and the Raman spectra were averaged for 60 acquisitions under the same conditions for better signal-to-noise ratios. The protein supernatant was dropped on the surface of the glass sheet wrapped in aluminized paper and quickly dried in a vacuum desiccator at room temperature. Here, the employment of aluminized paper can effectively

https://doi.org/10.1021/acsomega.3c01606
ACS Omega 2023, 8, 24999−25008

enhance the Raman signal of the protein.[51,52] Three different areas of each sample were selected for the measurement. The infrared spectrum was recorded on Nicolet iS50 FT-IR (Thermo Scientific, American). The protein solution was freeze-dried and mixed with potassium bromide for infrared detection. All measurements were performed three times under ambient conditions.

■ ASSOCIATED CONTENT

Supporting Information

The Supporting Information is available free of charge at https://pubs.acs.org/doi/10.1021/acsomega.3c01606.

> Size statistics of HEWL aggregates under different reaction conditions; size change of HEWL oligomers; comparison of ThT fluorescence kinetic curves under 5, 45, and 85 °C of ATs; Raman spectra of lyophilized HEWL at the native state and the state after 120 h of incubation with lower AT and higher AT; infrared spectra of lyophilized HEWL at the native state and the state after 120 h of incubation with lower AT and higher AT; assessment of the influence of temperature gradient; state of remaining samples in the glass vials after HEWL incubation for 24 h with lower AT and higher AT; characterization of hydrogels by AFM and spectroscopy; and remaining samples in the glass vials after HEWL incubation with lower AT and higher AT with gel (PDF)

■ AUTHOR INFORMATION

Corresponding Authors

Lei Xing − *State Key Laboratory of Analytical Chemistry for Life Science, School of Chemistry and Chemical Engineering, Nanjing University, Nanjing 210023, PR China;* orcid.org/0000-0003-4515-118X; Email: xl1992@nju.edu.cn

Jing-Juan Xu − *State Key Laboratory of Analytical Chemistry for Life Science, School of Chemistry and Chemical Engineering, Nanjing University, Nanjing 210023, PR China;* orcid.org/0000-0001-9579-9318; Email: xujj@nju.edu.cn

Authors

Han-Zhang Mou − *State Key Laboratory of Analytical Chemistry for Life Science, School of Chemistry and Chemical Engineering, Nanjing University, Nanjing 210023, PR China*

Cong-Lin Zhao − *State Key Laboratory of Analytical Chemistry for Life Science, School of Chemistry and Chemical Engineering, Nanjing University, Nanjing 210023, PR China*

Juan Song − *State Key Laboratory of Analytical Chemistry for Life Science, School of Chemistry and Chemical Engineering, Nanjing University, Nanjing 210023, PR China*

Hong-Yuan Chen − *State Key Laboratory of Analytical Chemistry for Life Science, School of Chemistry and Chemical Engineering, Nanjing University, Nanjing 210023, PR China*

Complete contact information is available at: https://pubs.acs.org/10.1021/acsomega.3c01606

Author Contributions

The manuscript was written through the contributions of all authors. All authors have approved the final version of the manuscript.

Notes

The authors declare no competing financial interest.

■ ACKNOWLEDGMENTS

We gratefully acknowledge the financial support from the National Natural Science Foundation of China (21991080 and 21327902), the Excellent Research Program of Nanjing University (ZYJH004), and the China Postdoctoral Science Foundation (2019TQ0145).

■ REFERENCES

(1) Li, J.; Zhang, F. Amyloids as Building Blocks for Macroscopic Functional Materials: Designs, Applications and Challenges. *Int. J. Mol. Sci.* **2021**, *22*, 10698.

(2) Lopez-Silva, T. L.; Schneider, J. P. From structure to application: Progress and opportunities in peptide materials development. *Curr. Opin. Chem. Biol.* **2021**, *64*, 131−144.

(3) Mason, T. O.; Shimanovich, U. Fibrous Protein Self-Assembly in Biomimetic Materials. *Adv. Mater.* **2018**, *30*, No. e1706462.

(4) Wei, G.; Su, Z.; Reynolds, N. P.; Arosio, P.; Hamley, I. W.; Gazit, E.; Mezzenga, R. Self-assembling peptide and protein amyloids: from structure to tailored function in nanotechnology. *Chem. Soc. Rev.* **2017**, *46*, 4661−4708.

(5) Chiti, F.; Dobson, C. M. Protein misfolding, functional amyloid, and human disease. *Annu. Rev. Biochem.* **2006**, *75*, 333−366.

(6) Dobson, C. M. Protein folding and misfolding. *Nature* **2003**, *426*, 884−890.

(7) Hamley, I. W. Peptide fibrillization. *Angew. Chem., Int. Ed.* **2007**, *46*, 8128−8147.

(8) Kayser, J. J.; Arnold, P.; Steffen-Heins, A.; Schwarz, K.; Keppler, J. K. Functional ethanol-induced fibrils: Influence of solvents and temperature on amyloid-like aggregation of beta-lactoglobulin. *J. Food Eng.* **2020**, *270*, 109764.

(9) Das, S.; Jacob, R. S.; Patel, K.; Singh, N.; Maji, S. K. Amyloid fibrils: versatile biomaterials for cell adhesion and tissue engineering applications. *Biomacromolecules* **2018**, *19*, 1826−1839.

(10) Chen, Y.; Liu, Q.; Yang, F.; Yu, H.; Xie, Y.; Yao, W. Lysozyme amyloid fibril: Regulation, application, hazard analysis, and future perspectives. *Int. J. Biol. Macromol.* **2022**, *200*, 151−161.

(11) Chen, D.; Pinho, L. S.; Federici, E.; Zuo, X.; Ilavsky, J.; Kuzmenko, I.; Yang, Z.; Jones, O. G.; Campanella, O. Heat accelerates degradation of *β*-lactoglobulin fibrils at neutral pH. *Food Hydrocolloids* **2022**, *124*, 107291.

(12) Shimanovich, U.; Efimov, I.; Mason, T. O.; Flagmeier, P.; Buell, A. K.; Gedanken, A.; Linse, S.; Akerfeldt, K. S.; Dobson, C. M.; Weitz, D. A.; et al. Protein Microgels from Amyloid Fibril Networks. *ACS Nano* **2015**, *9*, 43−51.

(13) Swaminathan, R.; Ravi, V. K.; Kumar, S.; Kumar, M. V. S.; Chandra, N. Lysozyme: a model protein for amyloid research. *Adv. Protein Chem. Struct. Biol.* **2011**, *84*, 63−111.

(14) Frachon, T.; Bruckert, F.; Le Masne, Q.; Monnin, E.; Weidenhaupt, M. Insulin Aggregation at a Dynamic Solid-Liquid-Air Triple Interface. *Langmuir* **2016**, *32*, 13009−13019.

(15) Kiran Kumar, E.; Prasad, D. K.; Prakash Prabhu, N. Concentration dependent switch in the kinetic pathway of lysozyme fibrillation: Spectroscopic and microscopic analysis. *Spectrochim. Acta, Part A* **2017**, *183*, 187−194.

(16) Campioni, S.; Bagnani, M.; Pinotsi, D.; Lecinski, S.; Rodighiero, S.; Adamcik, J.; Mezzenga, R. Interfaces Determine the Fate of Seeded *α*-Synuclein Aggregation. *Adv. Mater. Interfaces* **2020**, *7*, 2000446.

(17) Campioni, S.; Carret, G.; Jordens, S.; Nicoud, L.; Mezzenga, R.; Riek, R. The presence of an air-water interface affects formation and

elongation of alpha-Synuclein fibrils. *J. Am. Chem. Soc.* **2014**, *136*, 2866−2875.
(18) Brender, J. R.; Krishnamoorthy, J.; Sciacca, M. F.; Vivekanandan, S.; D'Urso, L.; Chen, J.; La Rosa, C.; Ramamoorthy, A. Probing the sources of the apparent irreproducibility of amyloid formation: drastic changes in kinetics and a switch in mechanism due to micellelike oligomer formation at critical concentrations of IAPP. *J. Phys. Chem. B* **2015**, *119*, 2886−2896.
(19) Jayamani, J.; Shanmugam, G. Diameter of the vial plays a crucial role in the amyloid fibril formation: Role of interface area between hydrophilic-hydrophobic surfaces. *Int. J. Biol. Macromol.* **2017**, *101*, 290−298.
(20) Toprakcioglu, Z.; Kamada, A.; Michaels, T. C. T.; Xie, M.; Krausser, J.; Wei, J.; Saric, A.; Vendruscolo, M.; Knowles, T. P. J. Adsorption free energy predicts amyloid protein nucleation rates. *Proc. Natl. Acad. Sci. U. S. A.* **2022**, *119*, No. e2109718119.
(21) Zhou, X. M.; Shimanovich, U.; Herling, T. W.; Wu, S.; Dobson, C. M.; Knowles, T. P. J.; Perrett, S. Enzymatically Active Microgels from Self-Assembling Protein Nanofibrils for Microflow Chemistry. *ACS Nano* **2015**, *9*, 5772−5781.
(22) Kummer, N.; Wu, T.; De France, K. J.; Zuber, F.; Ren, Q.; Fischer, P.; Campioni, S.; Nystrom, G. Self-Assembly Pathways and Antimicrobial Properties of Lysozyme in Different Aggregation States. *Biomacromolecules* **2021**, *22*, 4327−4336.
(23) Khan, A. N.; Khan, R. H. Protein misfolding and related human diseases: A comprehensive review of toxicity, proteins involved, and current therapeutic strategies. *Int. J. Biol. Macromol.* **2022**, *223*, 143−160.
(24) Xing, L.; Fan, W.; Chen, N.; Li, M.; Zhou, X.; Liu, S. Amyloid formation kinetics of hen egg white lysozyme under heat and acidic conditions revealed by Raman spectroscopy. *J. Raman Spectrosc.* **2019**, *50*, 629−640.
(25) Xing, L.; Lin, K.; Zhou, X.; Liu, S.; Luo, Y. Multistate Mechanism of Lysozyme Denaturation through Synchronous Analysis of Raman Spectra. *J. Phys. Chem. B* **2016**, *120*, 10660−10667.
(26) Huyst, A. M. R.; Deleu, L. J.; Luyckx, T.; Buyst, D.; Van Camp, J.; Delcour, J. A.; Van der Meeren, P. Colloidal stability of oil-in-water emulsions prepared from hen egg white submitted to dry and/or wet heating to induce amyloid-like fibril formation. *Food Hydrocolloids* **2022**, *125*, 107450.
(27) Knowles, T. P.; Mezzenga, R. Amyloid Fibrils as Building Blocks for Natural and Artificial Functional Materials. *Adv. Mater.* **2016**, *28*, 6546−6561.
(28) Fan, W.; Xing, L.; Chen, N.; Zhou, X.; Yu, Y.; Liu, S. Promotion Effect of Succinimide on Amyloid Fibrillation of Hen Egg-White Lysozyme. *J. Phys. Chem. B* **2019**, *123*, 8057−8064.
(29) Xing, L.; Chen, N.; Fan, W.; Li, M.; Zhou, X.; Liu, S. Double-edged effects of aluminium ions on amyloid fibrillation of hen egg-white lysozyme. *Int. J. Biol. Macromol.* **2019**, *132*, 929−938.
(30) Adamcik, J.; Mezzenga, R. Study of amyloid fibrils via atomic force microscopy. *Curr. Opin. Colloid Interface Sci.* **2012**, *17*, 369−376.
(31) Krebs, M. R.; Bromley, E. H.; Donald, A. M. The binding of thioflavin-T to amyloid fibrils: localisation and implications. *J. Struct. Biol.* **2005**, *149*, 30−37.
(32) Sebastiao, M.; Quittot, N.; Bourgault, S. Thioflavin T fluorescence to analyse amyloid formation kinetics: Measurement frequency as a factor explaining irreproducibility. *Anal. Biochem.* **2017**, *532*, 83−86.
(33) Yan, M.; Wang, X. Study on the kinetic self-assembly of type I collagen from tilapia (Oreochromis niloticus) skin using the fluorescence probe thioflavin T. *Spectrochim. Acta, Part A* **2018**, *203*, 342−347.
(34) Heyn, T. R.; Mayer, J.; Neumann, H. R.; Selhuber-Unkel, C.; Kwade, A.; Schwarz, K.; Keppler, J. K. The threshold of amyloid aggregation of beta-lactoglobulin: Relevant factor combinations. *J. Food Eng.* **2020**, *283*, 110005.
(35) Ow, S. Y.; Dunstan, D. E. The effect of concentration, temperature and stirring on hen egg white lysozyme amyloid formation. *Soft Matter* **2013**, *9*, 9692−9701.
(36) Shashilov, V. A.; Lednev, I. K. 2D correlation deep UV resonance raman spectroscopy of early events of lysozyme fibrillation: kinetic mechanism and potential interpretation pitfalls. *J. Am. Chem. Soc.* **2008**, *130*, 309−317.
(37) Khan, J. M.; Malik, A.; Sen, P.; Ahmed, A.; Ahmed, M.; Alamery, S. F.; Almaharfi, H. A.; Choudhry, H.; Khan, M. I. Different conformational states of hen egg white lysozyme formed by exposure to the surfactant of sodium dodecyl benzenesulfonate. *Int. J. Biol. Macromol.* **2019**, *128*, 54−60.
(38) Rygula, A.; Majzner, K.; Marzec, K. M.; Kaczor, A.; Pilarczyk, M.; Baranska, M. Raman spectroscopy of proteins: a review. *J. Raman Spectrosc.* **2013**, *44*, 1061−1076.
(39) Shashilov, V.; Xu, M.; Ermolenkov, V. V.; Fredriksen, L.; Lednev, I. K. Probing a fibrillation nucleus directly by deep ultraviolet Raman spectroscopy. *J. Am. Chem. Soc.* **2007**, *129*, 6972−6973.
(40) Shashilov, V. A.; Xu, M.; Ermolenkov, V. V.; Lednev, I. K. Latent variable analysis of Raman spectra for structural characterization of proteins. *J. Quant. Spectrosc. Radiat. Transfer* **2006**, *102*, 46−61.
(41) Xu, M.; Ermolenkov, V. V.; He, W.; Uversky, V. N.; Fredriksen, L.; Lednev, I. K. Lysozyme fibrillation: deep UV Raman spectroscopic characterization of protein structural transformation. *Biopolymers* **2005**, *79*, 58−61.
(42) Spiro, T. G.; Gaber, B. P. Laser Raman scattering as a probe of protein structure. *Annu. Rev. Biochem.* **1977**, *46*, 553−570.
(43) Wen, Z. Q. Raman spectroscopy of protein pharmaceuticals. *J. Pharm. Sci.* **2007**, *96*, 2861−2878.
(44) Chen, M. C.; Lord, R. C.; Mendelsohn, R. Laser-Excited Raman Spectroscopy of Biomolecules.V. Conformational Changes Associated with the Chemical Denaturation of Lysozyme. *J. Am. Chem. Soc.* **1974**, *96*, 3038−3042.
(45) Sassi, P.; Giugliarelli, A.; Paolantoni, M.; Morresi, A.; Onori, G. Unfolding and aggregation of lysozyme: A thermodynamic and kinetic study by FTIR spectroscopy. *Biophys. Chem.* **2011**, *158*, 46−53.
(46) Zou, Y.; Li, Y.; Hao, W.; Hu, X.; Ma, G. Parallel β-Sheet Fibril and Antiparallel β-Sheet Oligomer: New Insights into Amyloid Formation of Hen Egg White Lysozyme under Heat and Acidic Condition from FTIR Spectroscopy. *J. Phys. Chem. B* **2013**, *117*, 4003−4013.
(47) Oladepo, S. A.; Xiong, K.; Hong, Z.; Asher, S. A.; Handen, J.; Lednev, I. K. UV Resonance Raman Investigations of Peptide and Protein Structure and Dynamics. *Chem. Rev.* **2012**, *112*, 2604−2628.
(48) Kurouski, D.; Van Duyne, R. P.; Lednev, I. K. Exploring the structure and formation mechanism of amyloid fibrils by Raman spectroscopy: a review. *Analyst* **2015**, *140*, 4967−4980.
(49) Krausser, J.; Knowles, T. P. J.; Saric, A. Physical mechanisms of amyloid nucleation on fluid membranes. *Proc. Natl. Acad. Sci. U.S.A.* **2020**, *117*, 33090−33098.
(50) Tornquist, M.; Michaels, T. C. T.; Sanagavarapu, K.; Yang, X.; Meisl, G.; Cohen, S. I. A.; Knowles, T. P. J.; Linse, S. Secondary nucleation in amyloid formation. *Chem. Commun.* **2018**, *54*, 8667−8684.
(51) Tian, S.; Neumann, O.; McClain, M. J.; Yang, X.; Zhou, L.; Zhang, C.; Nordlander, P.; Halas, N. J. Aluminum Nanocrystals: A Sustainable Substrate for Quantitative SERS-Based DNA Detection. *Nano Lett.* **2017**, *17*, 5071−5077.
(52) Su, D.; Jiang, S.; Yu, M.; Zhang, G.; Liu, H.; Li, M.-Y. Facile fabrication of configuration controllable self-assembled Al nanostructures as UV SERS substrates. *Nanoscale* **2018**, *10*, 22737−22744.

https://doi.org/10.1021/acsomega.3c01606
ACS Omega 2023, 8, 24999−25008